Hindawi Publishing Corporation
International Journal of Photoenergy
Volume 2016, Article ID 2124087, 10 pages
http://dx.doi.org/10.1155/2016/2124087

Research Article

Adhesion Improvement and Characterization of Magnetron Sputter Deposited Bilayer Molybdenum Thin Films for Rear Contact Application in CIGS Solar Cells

Weimin Li,[1,2] Xia Yan,[1,3] Armin G. Aberle,[1,2,3] and Selvaraj Venkataraj[1]

[1]*Solar Energy Research Institute of Singapore, National University of Singapore, Singapore 117574*
[2]*Department of Electrical and Computer Engineering, National University of Singapore, Singapore 117576*
[3]*NUS Graduate School for Integrative Sciences & Engineering (NGS), National University of Singapore, 28 Medical Drive, Singapore 117456*

Correspondence should be addressed to Selvaraj Venkataraj; s.venkataraj@nus.edu.sg

Received 23 March 2016; Accepted 28 June 2016

Academic Editor: Sergey Varlamov

Molybdenum (Mo) thin films are widely used as rear electrodes in copper indium gallium diselenide (CIGS) solar cells. The challenge in Mo deposition by magnetron sputtering lies in simultaneously achieving good adhesion to the substrates while retaining the electrical and optical properties. Bilayer Mo films, comprising five different thickness ratios of a high pressure (HP) deposited bottom layer and a low pressure (LP) deposited top layer, were deposited on 40 cm × 30 cm soda-lime glass substrates by DC magnetron sputtering. We focus on understanding the effects of the individual layer properties on the resulting bilayer Mo films, such as microstructure, surface morphology, and surface oxidation. We show that the thickness of the bottom HP Mo layer plays a major role in determining the micromechanical and physical properties of the bilayer Mo stack. Our studies reveal that a thicker HP Mo bottom layer not only improves the adhesion of the bilayer Mo, but also helps to improve the film crystallinity along the preferred [110] direction. However, the surface roughness and the porosity of the bilayer Mo films are found to increase with increasing bottom layer thickness, which leads to lower optical reflectance and a higher probability for oxidation at the Mo surface.

1. Introduction

Copper indium gallium diselenide [Cu(In,Ga)Se_2 or CIGS] based solar cells are one of the most attractive thin-film photovoltaic (PV) technologies, due to their potential to achieve high efficiency [1]. Recently, ZSW in Germany has reported a record efficiency of 21.7% [2], which has surpassed that of the market-dominating multicrystalline silicon wafer based solar cells (20.8%) [1, 3]. Due to the very high optical absorption coefficient of CIGS solar cells (of the order of 10^5 cm^{-1} for photons with energies above 1 eV), a very thin absorber layer (2-3 μm) is sufficient to absorb almost all of the incident solar photons, which enables decreasing the raw material usage and reducing the fabrication cost [3, 4]. Moreover, CIGS thin-film solar cells can also be fabricated on almost any kind of substrate, such as flexible polyethylene terephthalate (PET) foils, stainless steel substrates, and rigid glass sheets [5]. The use of glass substrates has the potential to further reduce the production costs. In addition to rooftop applications, CIGS solar cells can also be used in space [6].

The first step in making CIGS solar cells is to deposit a metallic rear contact. Since the rear contact is the first functional layer in a CIGS solar cell, its quality plays a major role in the overall performance of the device. There are many requirements for the rear contact in CIGS solar cells, including the following: (1) low electrical resistivity, (2) good adhesion to the substrate, (3) high optical reflectance, (4) columnar structure for alkali (Na) diffusion when soda-lime glass (SLG) is used as the substrate, (5) formation of an ohmic contact with the p-type CIGS absorber layer, and (6) high stability during the corrosive selenization process at 500 to 550°C to form the CIGS absorber layer [7–10]. Various metals were studied in the literature as rear contact for CIGS solar cells, including Au, Ag, Ni, Mo, Ti, Cu, and

Al [11–17]. Among these investigated materials, magnetron sputter deposited molybdenum (Mo) is the best choice for forming the rear contact of CIGS solar cells, because of its low electrical resistivity, high stability against corrosive environments, and low contact resistance with the CIGS layer by the formation of a thin $MoSe_2$ interlayer [18, 19]. However, the microstructure of the Mo layer not only greatly affects the formation of $MoSe_2$ at the Mo and CIGS interface during the high-temperature selenization process [20, 21], but also determines the layer-to-layer adhesion (SLG substrate, Mo rear contact, and CIGS absorber) [22]. It is therefore critical to tailor the properties of the Mo rear contact to fulfil these requirements and to achieve high-efficiency CIGS solar cells.

The properties of magnetron sputter deposited Mo rear contacts greatly depend on the deposition parameters, especially the power applied to the Mo target and the chamber pressure [23, 24]. At relatively low deposition pressure, the Mo film exhibits a dense morphology and low electrical resistivity, but with intrinsic compressive strain and thus poor adhesion to the substrate; in contrast, at relatively high deposition pressure, the film shows a porous morphology and a high electrical resistivity with intrinsic tensile strain but good adhesion to the substrate [25–27]. Thus, it is a challenge to fabricate single-layer Mo films with both low resistivity and good adhesion to the substrate [28]. One conventional method to solve this problem is to fabricate Mo bilayer films which consist of a high pressure deposited bottom layer (to obtain good adhesion) and a low pressure deposited top layer (to maintain low electrical resistivity).

Several groups have reported the deposition of Mo bilayer stacks for rear electrode applications in CIGS solar cells [25, 29–33]. The most widely studied topic is to find the balance between good adhesion and low electrical resistivity. However, there are only very few studies about the influence of the properties of the individual layers on the performance of bilayer Mo films [25, 29–34]. Salomé et al. reported the optimization of Mo bilayers [33]. They varied the bottom Mo layer thickness to achieve good adhesion, but the overall thickness of the Mo stack was different for each deposition condition [33]. In addition, Mo rear contacts were found to degrade over time due to surface oxidation, which leads to the degradation of the whole device [35, 36]. Hence, in the present study, we make an attempt to prepare bilayer Mo films comprising different thickness ratios of high pressure deposited bottom layers (HP Mo) and low pressure deposited top layers (LP Mo) while keeping the total layer thickness constant (~900 nm). We focus on developing an improved understanding of the effects of the individual layer thicknesses on the overall properties of bilayer Mo films, such as microstructure, surface morphology, and surface oxidation. Based on the characterization and analysis of experimental samples, we establish a reliable method to deposit durable bilayer Mo films that are well suited as rear contacts of CIGS solar cells.

2. Experimental Details

Mo films were deposited onto 3 mm thick soda-lime glass (SLG) substrates by direct current (DC) magnetron sputtering (FHR Line 540 from FHR Anlagenbau GmbH, Germany) using a planar Mo target (size: 9 cm × 51 cm, purity: 99.999%). The glass substrates were cleaned by a laboratory glassware washer (Miele, G7883CD) using alkaline detergent and then cleaned by three cycles of deionized (DI) water rinse procedure. After cleaning, the glass was dried at 99°C for 25 minutes. The power applied to the target was kept constant at 2.0 kW. The chamber pressure was controlled by adjusting the Ar gas flow: 330 sccm at 6.0×10^{-3} mbar (high pressure, HP) and 50 sccm at 1.5×10^{-3} mbar (low pressure, LP). All films were deposited at room temperature conditions. The total thickness of the bilayer Mo stacks was kept constant at about 900 nm. Bilayer stacks with five different thickness ratios of a HP deposited Mo bottom layer and a LP deposited Mo top layer were deposited under identical conditions, as shown in Figure 1. The thickness of the Mo layers was adjusted by varying the number of oscillations ("passes") of the substrate holder in front of the glowing sputter cathode. In addition, for the purpose of sample characterization and comparison, single-layer Mo films with a thickness of about 90 nm and 900 nm were also deposited at both HP and LP.

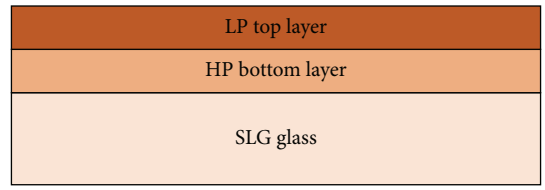

Figure 1: Schematic of the bilayer Mo rear electrode design. The bottom Mo layer was deposited at HP (6.0×10^{-3} mbar) while the top Mo layer was deposited at LP (1.5×10^{-3} mbar). The total thickness of the bilayer Mo stacks was approximately 900 nm.

X-ray reflectivity (XRR) measurements were carried out on the ~90 nm thick single-layer Mo films (HP and LP) by high-resolution specular X-ray reflectometry (XRR) at grazing incidence. These measurements were performed in the X-ray demonstration and development (XDD) beam line facility at the Singapore Synchrotron Light Source (SSLS). The density, roughness, and thickness of the films were derived by simulations of the measured XRR curves. The thickness of the ~900 nm thick Mo films was confirmed with a stylus profiler (Dektak from Bruker). The total thickness of the investigated films was in the 883–903 nm range. The sheet resistance of the films was measured with a four-point probe in the van der Pau configuration. The adhesion of the Mo films to the substrates was examined with a standard Scotch tape test [23, 25]. The crystal structure of the films was characterized with an X-ray diffractometer (XRD, model Bruker D8 diffractometer). The grazing angle geometry was used to record the XRD patterns of the 900 nm thick Mo films. This method is very sensitive to the surface structure of a thin film. The surface morphologies of the Mo films were investigated by scanning electron microscopy (SEM) and atomic force microscopy (AFM). The optical reflectance of the samples in the visible region was measured by UV-Vis spectrometry. In order to examine the long-term stability of the bilayer Mo films,

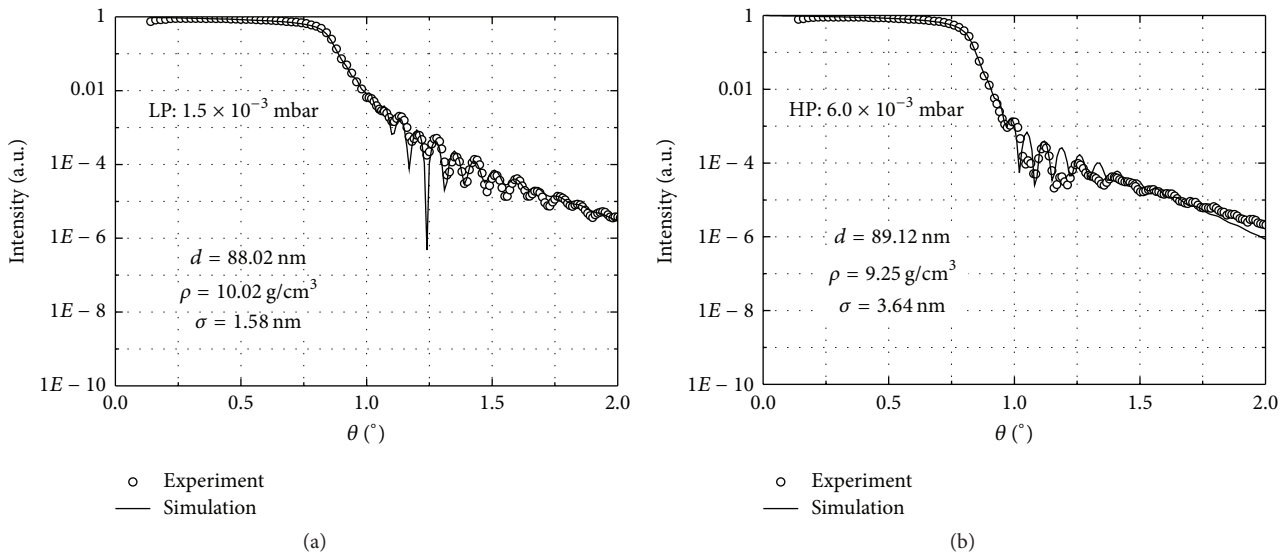

Figure 2: XRR measurements of single-layer Mo films of thickness ~90 nm deposited at (a) low pressure (1.5×10^{-3} mbar) and (b) high pressure (6×10^{-3} mbar).

Raman scattering was used to measure the surface oxidation of the films three months after the preparation of the samples.

3. Results and Discussion

3.1. X-Ray Reflectivity Measurement of Single-Layer Mo Films. XRR is a nondestructive and noncontact technique for the determination of film thicknesses in the 2–200 nm range, with precision of <3 Å. In addition, this technique can also be used to determine the density and interface roughness of films (even for multilayer stacks). XRR measurements were carried out for single-layer Mo films deposited at LP (1.5×10^{-3} mbar) and HP (6.0×10^{-3} mbar) conditions. Figure 2 depicts the XRR measurement curves recorded for these ~90 nm thick single-layer Mo films. The experimental curves are fitted using a software package to derive the film properties such as thickness, density, and roughness. As shown in Figure 2, the simulated curves fit the measured curves quite well, and hence, the film properties are derived with high accuracy. When comparing Figures 2(a) and 2(b), it can be seen that the oscillation amplitude of the Mo film deposited at HP decays rapidly; this is an indication of high surface roughness for the films deposited at HP. We observed that the sample deposited at LP possesses a high density (10.02 g/cm^3), which is close to the bulk density of Mo (10.2 g/cm^3), and a very smooth surface with root mean square (RMS) roughness of 1.58 nm. In contrast, the film deposited at HP has a low density (9.25 g/cm^3) and relatively high surface roughness (3.64 nm). This observation can be attributed to the energy differences of the sputtered particles arriving on the SLG substrate at different deposition pressures: at higher deposition pressure, the sputtered particles will have more collisions with the Ar gas molecules, which leads to a reduced kinetic energy when arriving at the substrate surface. Due to the reduced kinetic energy, the film deposited at HP has a more porous structure and a rougher surface. In contrast, at low deposition pressure, there are fewer collisions with the Ar gas molecules, and thus the arriving particles have a higher kinetic energy that is available for the rearrangement of the atoms at the surface. This in turn results in a denser film structure and a smoother film surface [37].

3.2. Crystallinity and Microstructure. The crystalline structure of the Mo rear electrode stacks was studied by XRD measurements in the grazing angle setup. All samples were measured at a fixed inclination angle of 2° and the XRD spectra were recorded from 20 to 75°. From the measurements, we found two pronounced peaks centered at 2θ = 40.5° and 73.7° (see Figure 3). These two peaks are indexed to Mo (110) and Mo (211), respectively. It should be noted that the single-layer Mo film deposited at LP (Figure 3(a)) has a better crystallinity with a stronger and sharper peak at 2θ = 40.5° compared to the single-layer Mo film deposited at HP (Figure 3(b)). This can be attributed to the higher kinetic energy of the sputtered particles at LP. In addition, the Mo (110) peak at 2θ = 40.5° also shows a slight shift towards lower angles as the deposition pressure is increased from 1.5×10^{-3} to 6.0×10^{-3} mbar, due to the changes in the deposition induced built-in stress levels within the films (which change from the compressive to the tensile state) caused by the different densities of the films (as measured by XRR; see Figure 2). All bilayer samples crystallized preferably along the [110] direction, which is a typical feature for the body-centered cubic (BCC) crystal structure of metallic Mo. This is due to the highest planar density and the minimum surface free energy of the (110) planes of the BBC crystal structure [22]. As shown in the literature [38–40], (110) planes are more favorable for preparing high-efficiency CIGS solar cells. Previous studies showed that the (110)-oriented single-crystal Mo rear contacts can enhance the (220) and (204) orientations of the CIGS absorber layer and thus significantly reduce grain boundary recombination losses in CIGS solar

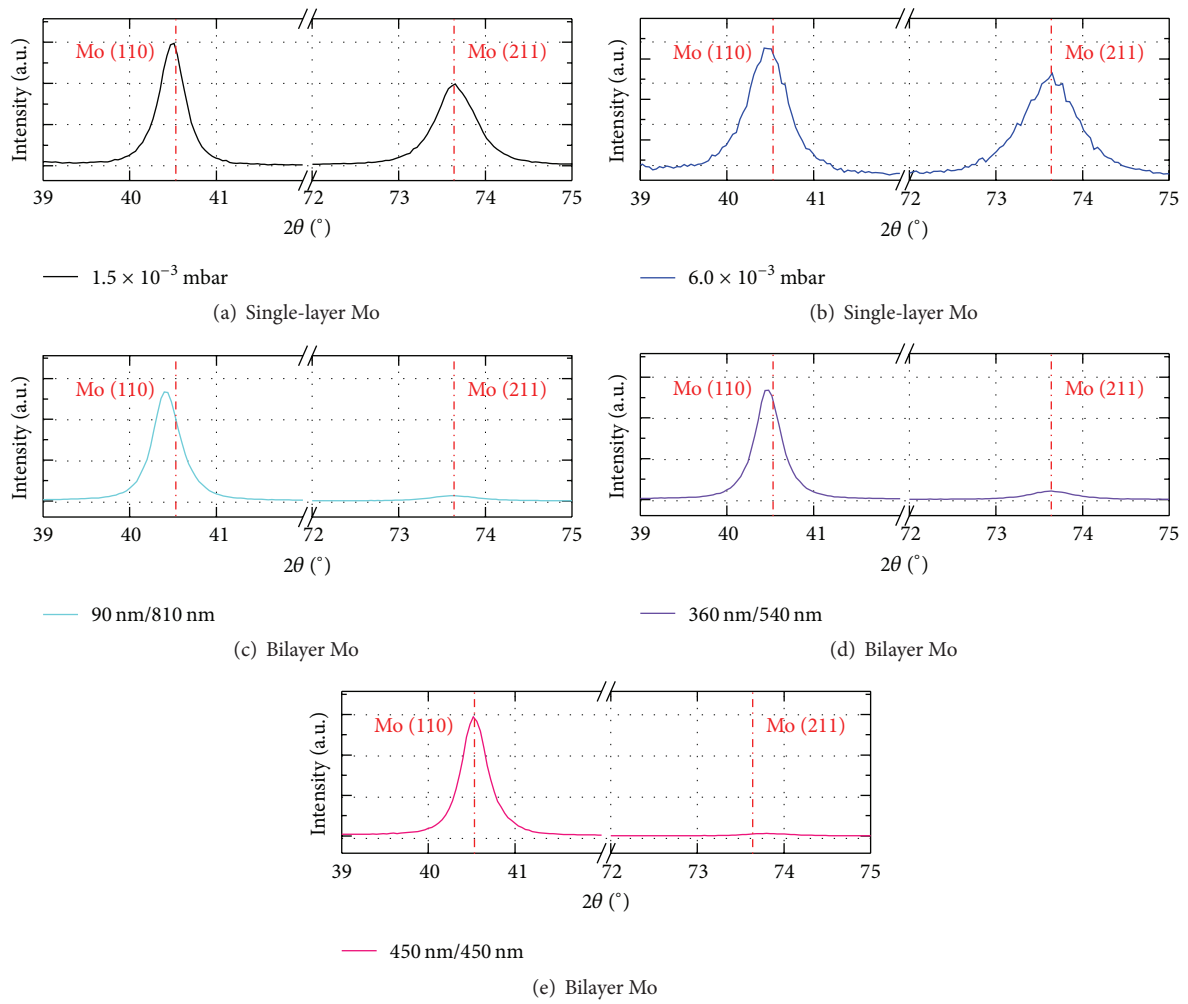

Figure 3: XRD patterns of single-layer and bilayer Mo films. The scanning range is centered at the Mo (110) and Mo (211) lattice planes.

cells, leading to the improved photovoltaic efficiency of CIGS solar cells [38–40].

The effects of the thickness of the bottom layer Mo film on the full width at half maximum (FWHM) and grain size of bilayer Mo films are illustrated in Figure 4. The grain size was calculated via the Scherrer equation:

$$\text{Grain size}\,(D) = \frac{0.9\lambda}{\beta \cos\theta}, \tag{1}$$

where λ, β, and θ are the wavelength of the X-rays ($K\alpha_1$), the FWHM, and the Bragg diffraction angle, respectively. Figure 4 shows that the FWHM increases and the grain size decreases with increasing bottom layer thickness. This is related to the small crystalline size of the bottom Mo films deposited at high pressure and the large FWHM of the Mo (110) peak. When the thickness of the bottom layer increases from 90 to 450 nm, the grain size of the bilayer Mo films decreases from 24.5 nm to 15.5 nm; this can be attributed to the smaller grain size of bottom HP Mo layers.

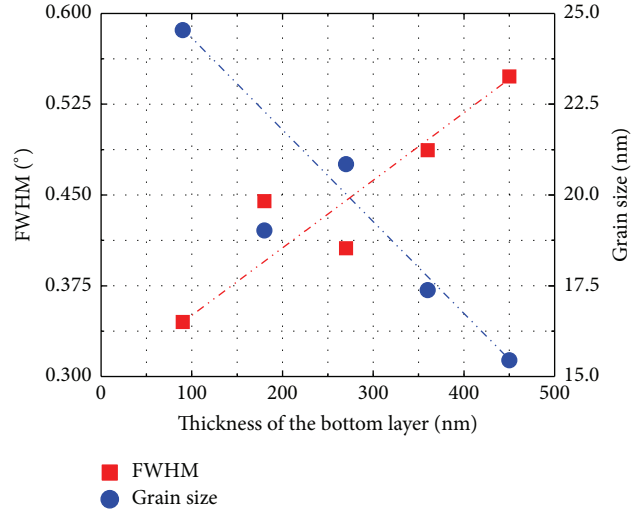

Figure 4: FWHM and grain size of bilayer Mo films as a function of the bottom layer thickness.

3.3. Surface Morphology. The surface morphology of the bilayer Mo films was studied by SEM and AFM. Figure 5 shows surface-view and cross-sectional SEM images of three Mo films deposited at different conditions. It can

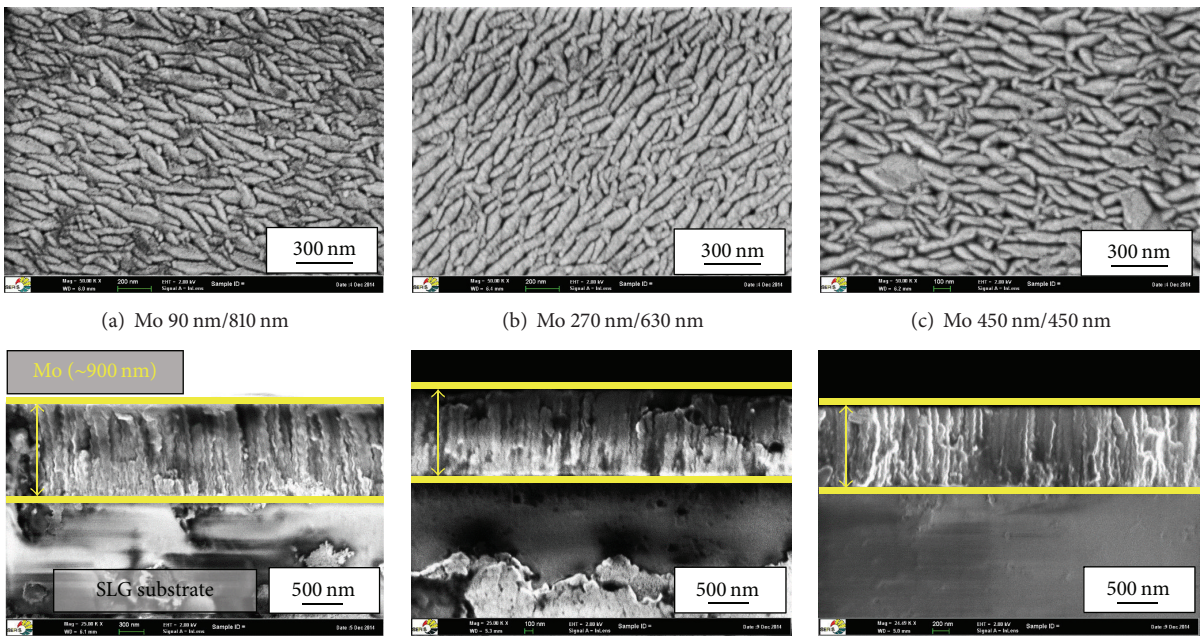

(a) Mo 90 nm/810 nm (b) Mo 270 nm/630 nm (c) Mo 450 nm/450 nm

(d) Mo 90 nm/810 nm (e) Mo 270 nm/630 nm (f) Mo 450 nm/450 nm

Figure 5: Surface-view and cross-sectional SEM images of bilayer Mo films with different thickness ratios of the bottom and top Mo layers: (a) 90 nm/810 nm, (b) 270 nm/630 nm, and (c) 450 nm/450 nm.

be clearly seen that all Mo films possess elongated grains with open boundaries, which is the typical appearance for Mo films deposited by magnetron sputtering [41]. In the cross-sectional SEM images of Figure 5, no clear boundary is observed between the Mo layers deposited at different pressures, which indicates that the columnar structure grows continuously irrespective of the change in deposition pressure. However, it is interesting to note that the size of the columnar structures and the overall grain size decrease with increasing thickness of the HP deposited bottom Mo layer, which agrees well with the XRD findings. In addition, the porosity of the films was found to increase with increasing bottom Mo layer thickness, which is a direct effect of the low density and the high roughness values of HP deposited Mo films (see the XRR measurements in Figure 2). Figure 6 shows the surface morphology of the films as measured by AFM. These measurements reveal that, with increasing bottom Mo layer thickness, the RMS roughness of the films gradually increases from 7.2 to 10.4 nm, but the increase was still within the acceptable limits [42, 43]. This increase can directly be attributed to the roughness of the bottom Mo layer (deposited at HP). The cross-sectional SEM measurement shows clear evidence for continuous growth of the columnar structure. Hence, it seems that the top Mo layer deposited at LP adopted the roughness of the HP deposited bottom Mo layer.

3.4. Electrical Resistivity and Adhesion. The electromechanical properties of the deposited Mo films are summarized in Table 1. For single-layer Mo films, the film deposited at LP shows a lower sheet resistance (0.31 ohms/sq), but it failed the tape test; in contrast, the film deposited at HP showed a significantly higher sheet resistance (0.84 ohms/sq), but it passed the tape test. The sheet resistance of the bilayer Mo films increased slightly with increasing thickness of the HP deposited bottom layer. However, an increasing thickness of the HP deposited bottom Mo layer improves the adhesion to the SLG substrate, and the stack successfully passes the adhesion tape test when the thickness of the HP deposited bottom Mo layer reaches ~360 nm. The adhesion improved further for the sample prepared with the 450 nm thick HP deposited bottom Mo layer. This optimized bilayer stack possesses a sheet resistance of 0.37 ohms/sq, which is comparable to commercially available Mo substrates and is also acceptable for rear contact applications in CIGS solar cells. The observed differences in the adhesion properties of the films are caused by the intrinsic strain, which in turn is related to the microstructure of the films. This observation is in agreement with the literature [28].

3.5. Optical Properties. In order to understand the optical properties of the single-layer and bilayer Mo films, their optical reflectance was measured from 300 to 800 nm, as shown in Figure 7. For the single-layer Mo films, the reflectance of the LP deposited film is higher than that of the HP deposited film. The differences in the reflectance of the films deposited at different chamber pressures can be attributed to the observed differences in the surface roughness and density values. As explained in Section 3.3, the surface roughness of the HP deposited Mo film was comparatively higher than that of the LP deposited film. The HP deposited film also possesses a low density and a high porosity (see the XRR measurements of Section 3.1), which leads to a further reduction in the optical reflectance of the Mo films [44]. The second Mo

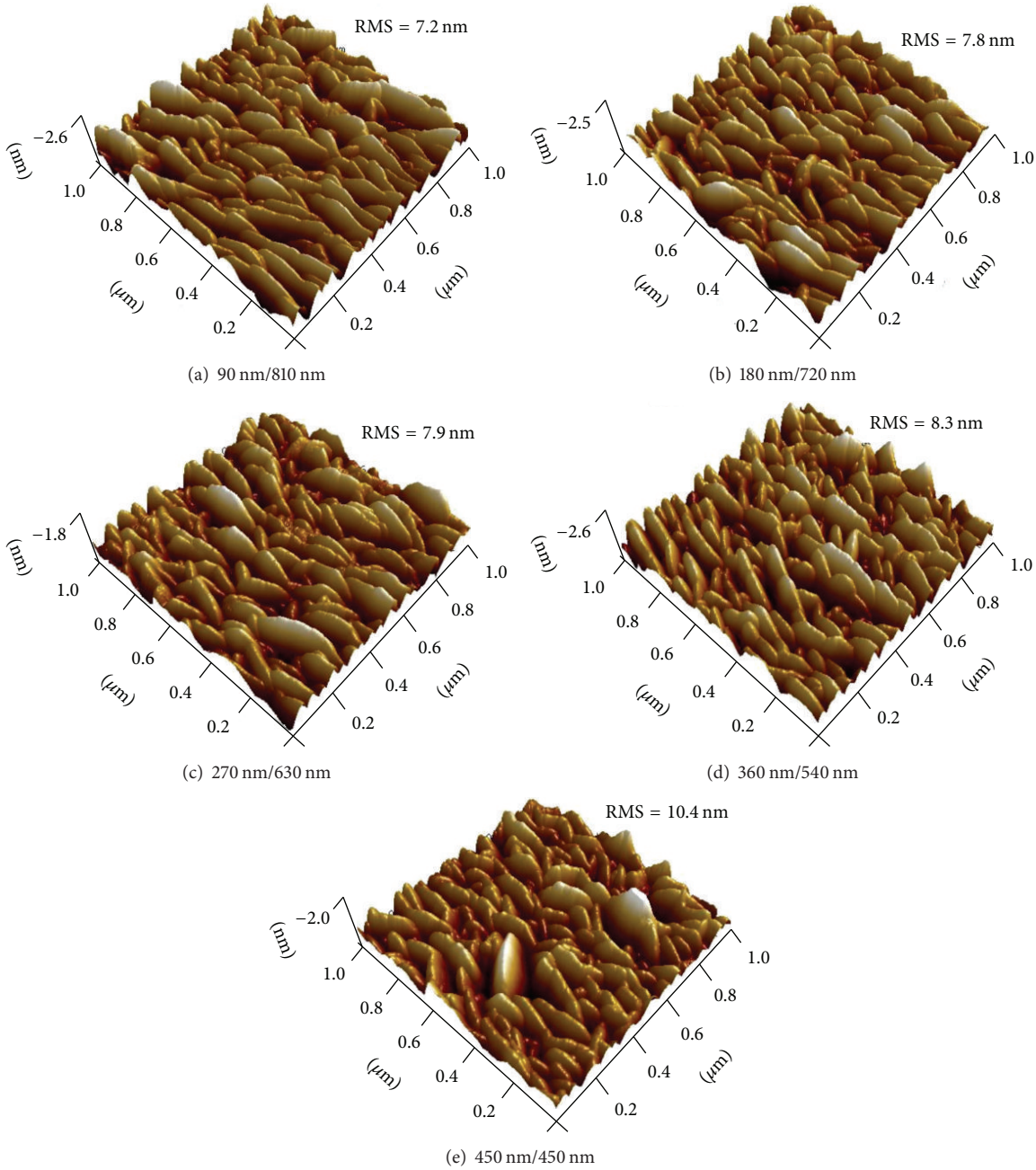

Figure 6: AFM 3D images of bilayer Mo stacks with different thickness ratios of bottom/top layers deposited on soda-lime glass substrates: (a) 90 nm/810 nm, (b) 180 nm/720 nm, (c) 270 nm/630 nm, (d) 360 nm/540 nm, and (e) 450 nm/450 nm.

film deposited at LP tends to conformally grow on the HP deposited Mo film, which has a rougher surface with more defects. Hence, the optical reflection of the bilayer Mo films decreases with increasing thickness of the HP deposited bottom Mo layer [44].

3.6. Raman Scattering Measurements. The surface oxidation of the Mo rear contact is critical in preparing high-efficiency CIGS solar cells. It has been reported that the oxygen adsorption on the surface is favorable for the diffusion of sodium atoms from the SLG substrate via the Mo rear contact into the CIGS absorber. However, the oxidation of the Mo rear contact was found to cause degradation issues of the Mo layer and thus to reduce the long-term stability of CIGS solar cells [45]. It is thus important to study the surface oxidation of Mo films and to correlate it to the microstructure properties.

In order to better understand the long-term stability of the Mo films prepared in this study, Raman measurements of the bilayer Mo films were carried out three months after the preparation of the films. The results are shown in Figure 8. Two weak peaks centered at 860 cm^{-1} and 958 cm^{-1} are observed in all samples, which correspond to the MoO_3

Table 1: Properties of 900 nm thick single-layer Mo films deposited at HP (6×10^{-3} mbar) and LP (1.5×10^{-3} mbar), as well as 900 nm thick bilayer Mo films consisting of different thickness ratios of the HP deposited bottom layer and the LP deposited top layer.

	Single-layer Mo films		Bilayer Mo stacks				
Sample number	HP	LP	(a)	(b)	(c)	(d)	(e)
Thickness of LP layer (nm)	900	0	810	720	630	540	450
Thickness of HP layer (nm)	0	900	90	180	270	360	450
Sheet resistance (ohm/sq)	0.84	0.31	0.31	0.32	0.32	0.36	0.37
Tape test (fail/pass)			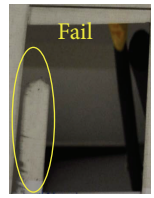			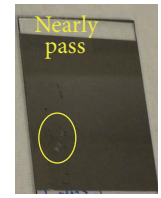	

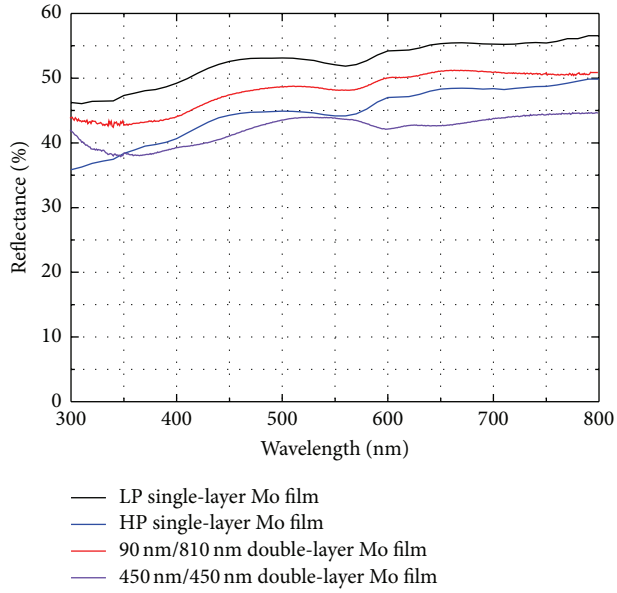

Figure 7: Measured optical reflectance of single-layer (LP and HP deposited) Mo films and bilayer Mo films (with 90 nm and 450 nm thick HP deposited bottom layer).

and Mo_8O_{23} modes. This confirms the formation of a thin oxide layer on the surface during the 3-month storage period. It is interesting to note that the intensity of the peak at 860 cm^{-1}, which corresponds to MoO_3, is increased when the thickness of the HP bottom Mo film is increased from 90 to 450 nm. This indicates the formation of oxide layers on the surfaces of the Mo films, whereby the oxide layer is thicker for the stacks with thicker HP deposited bottom Mo layer. The reason for the intensity variation of the MoO_x peaks is the increased adsorption of oxygen molecules at the porous surface structure, which in turn leads to a thicker surface oxide layer [45]. The XRR measurements reveal the porous nature of the HP deposited Mo films. The SEM and AFM surface morphology studies of Section 3.3 also confirmed the rough surface features of these Mo films. Hence, the increased surface oxidation can directly be attributed to defects at the surfaces of the Mo films deposited at HP.

4. Conclusion

The main intention of this study was to better understand the effects of the individual layer thicknesses on the properties of bilayer Mo stacks prepared for rear contact applications in CIGS thin-film solar cells. Bilayer Mo stacks with different thickness ratios of the bottom layer (deposited at high pressure: 6.0×10^{-3} mbar) and the top layer (deposited at low pressure: 1.5×10^{-3} mbar) were investigated. We found that the thickness of the bottom layer plays an important role for the micromechanical and physical properties of the bilayer stack. XRD and tape test studies revealed that a thicker bottom layer not only improves its adhesion to the glass substrate, but also enhances the film crystallinity and the growth of Mo grains with the preferred (110) orientation for high-efficiency CIGS solar cells. However, both the sheet resistance and the surface roughness of bilayer Mo stacks were found to increase with increasing bottom layer thickness. No boundary between the HP and LP deposited Mo layers was observed in cross-sectional SEM images, which implies a continuous growth of the Mo grains. The observed decrease in the optical reflectance is attributed to the increased surface roughness and decreased density of the films. The oxygen molecules adsorbed on the surface pores presumably act as nucleation centers to form a thin MoO_x surface oxide layer. Using Raman spectroscopy, the thickness of this oxide layer was found to increase with increasing bottom layer thickness. The bilayer Mo stacks on soda-lime glass developed in this work provide a highly durable and

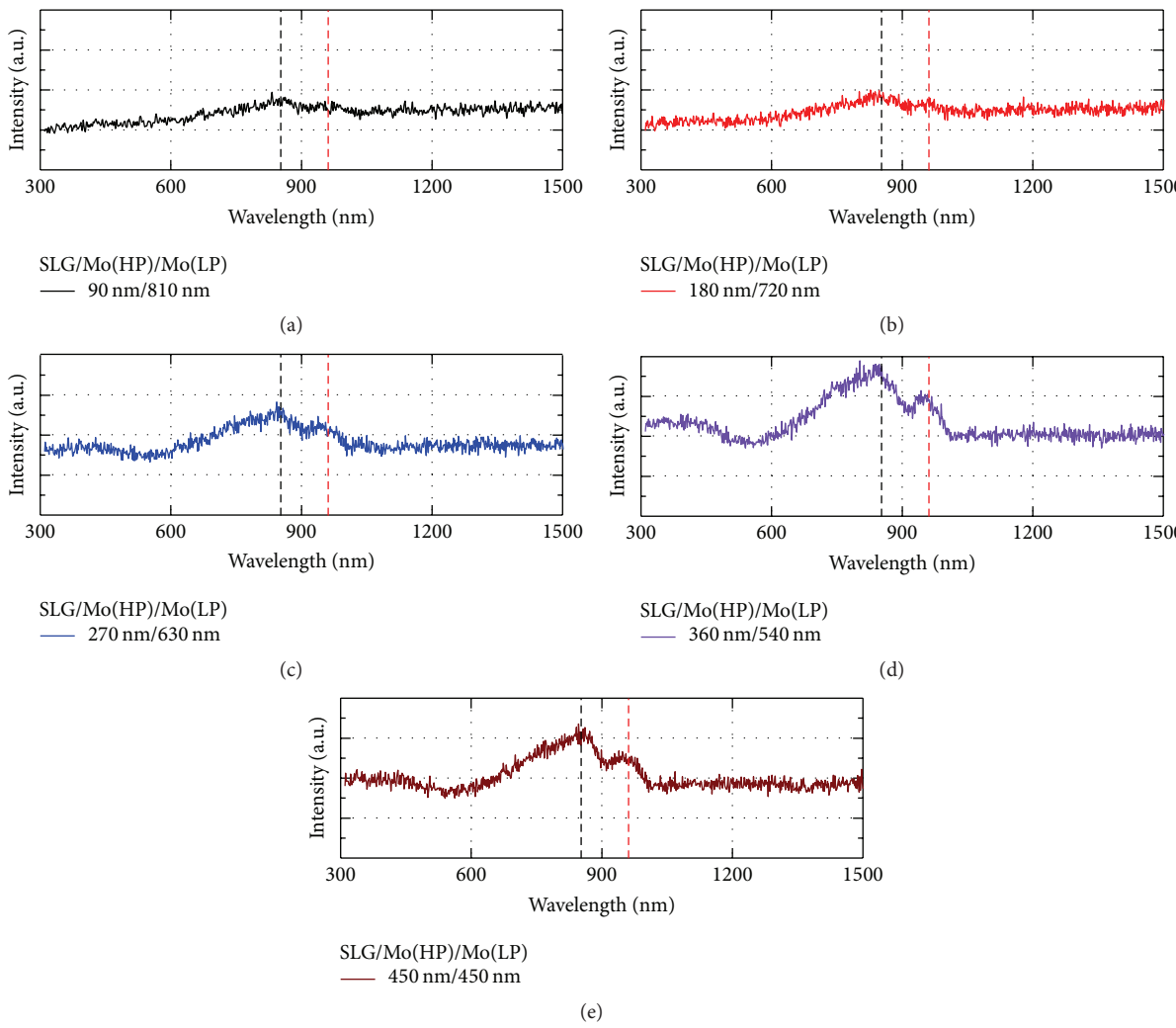

Figure 8: Raman spectra of bilayer Mo films with different thickness ratios of bottom layer and top layer.

low-resistance electrode that seems to be well suited as back contact of high-efficiency CIGS thin-film solar cells.

Competing Interests

The authors declare that they have no competing interests.

Acknowledgments

The Solar Energy Research Institute of Singapore (SERIS) is sponsored by the National University of Singapore (NUS) and the National Research Foundation (NRF) of Singapore through the Singapore Economic Development Board. This work was sponsored by NRF Grant NRF2011EWT-CERP001-019, "CIGS Solar Cells and Mini-Modules: Establishment of an R&D Pilot Line in Singapore and Associated Industry-Relevant Device Research." The X-ray reflectivity measurements were provided by the Singapore Synchrotron Light Source (SSLS) via NUS Core Support (C-380-003-003-001).

References

[1] M. A. Green, K. Emery, Y. Hishikawa, W. Warta, and E. D. Dunlop, "Solar cell efficiency tables (Version 45)," *Progress in Photovoltaics*, vol. 23, no. 1, pp. 1–9, 2015.

[2] P. Jackson, D. Hariskos, R. Wuerz et al., "Properties of Cu(In,Ga)Se_2 solar cells with new record efficiencies up to 21.7%," *Physica Status Solidi-Rapid Research Letters*, vol. 9, no. 1, pp. 28–31, 2015.

[3] P. Reinhard, F. Pianezzi, L. Kranz et al., "Flexible Cu(In,Ga)Se_2 solar cells with reduced absorber thickness," *Progress in Photovoltaics: Research and Applications*, vol. 23, no. 3, pp. 281–289, 2015.

[4] A. Rockett and R. W. Birkmire, "$CuInSe_2$ for photovoltaic applications," *Journal of Applied Physics*, vol. 70, no. 7, pp. R81–R97, 1991.

[5] A. Bosio, D. Menossi, G. Rosa, and N. Romeo, "Key developments in CIGS thin film solar cells on ceramic substrates," *Crystal Research and Technology*, vol. 49, no. 8, pp. 620–627, 2014.

[6] M. Günthner, M. Pscherer, C. Kaufmann, and G. Motz, "High emissivity coatings based on polysilazanes for flexible

$Cu(In,Ga)Se_2$ thin-film solar cells," *Solar Energy Materials and Solar Cells*, vol. 123, pp. 97–103, 2014.

[7] M. Powalla and B. Dimmler, "Scaling up issues of CIGS solar cells," *Thin Solid Films*, vol. 361, pp. 540–546, 2000.

[8] K. Orgassa, H. W. Schock, and J. H. Werner, "Alternative back contact materials for thin film $Cu(In,Ga)Se_2$ solar cells," *Thin Solid Films*, vol. 431-432, pp. 387–391, 2003.

[9] F. Kessler and D. Rudmann, "Technological aspects of flexible CIGS solar cells and modules," *Solar Energy*, vol. 77, no. 6, pp. 685–695, 2004.

[10] J. J. Scragg, J. T. Wätjen, M. Edoff, T. Ericson, T. Kubart, and C. Platzer-Björkman, "A detrimental reaction at the molybdenum back contact in $Cu_2ZnSn(S,Se)_4$ thin-film solar cells," *Journal of the American Chemical Society*, vol. 134, no. 47, pp. 19330–19333, 2012.

[11] R. V. Forest, E. Eser, B. E. Mccandless, R. W. Birkmire, and J. G. Chen, "Understanding the role of oxygen in the segregation of sodium at the surface of molybdenum coated soda-lime glass," *AIChE Journal*, vol. 60, no. 6, pp. 2365–2372, 2014.

[12] P. Blösch, S. Nishiwaki, T. Jaeger et al., "Alternative back contact designs for $Cu(In,Ga)Se_2$ solar cells on polyimide foils," *Thin Solid Films*, vol. 535, no. 1, pp. 220–223, 2013.

[13] T. Rissom, C. A. Kaufmann, R. Caballero, J. Schniebs, H.-W. Schock, and M. Wiedenbeck, "Influence of Mo back-contact oxidation on properties of $CIGSe_2$ thin film solar cells on glass substrates," *Japanese Journal of Applied Physics*, vol. 51, no. 10, Article ID 10NC02, 2012.

[14] Z. J. Li-Kao, N. Naghavi, F. Erfurth et al., "Towards ultrathin copper indium gallium diselenide solar cells: proof of concept study by chemical etching and gold back contact engineering," *Progress in Photovoltaics: Research and Applications*, vol. 20, no. 5, pp. 582–587, 2012.

[15] E. Moons, T. Engelhard, and D. Cahen, "Ohmic contacts to p-$CuInSe_2$ crystals," *Journal of Electronic Materials*, vol. 22, no. 3, pp. 275–280, 1993.

[16] C. L. Chan and I. Shih, "Al/p-$CuInSe_2$ metal-semiconductor contacts," *Journal of Applied Physics*, vol. 68, no. 1, pp. 156–160, 1990.

[17] R. J. Matson, O. Jamjoum, A. D. Buonaquisti et al., "Metal contacts to $CuInSe_2$," *Solar Cells*, vol. 11, no. 3, pp. 301–305, 1984.

[18] S. Niki, M. Contreras, I. Repins et al., "CIGS absorbers and processes," *Progress in Photovoltaics: Research and Applications*, vol. 18, no. 6, pp. 453–466, 2010.

[19] P. Bommersbach, L. Arzel, M. Tomassini et al., "Influence of Mo back contact porosity on co-evaporated $Cu(In,Ga)Se_2$ thin film properties and related solar cell," *Progress in Photovoltaics: Research and Applications*, vol. 21, no. 3, pp. 332–343, 2013.

[20] T. Wada, N. Kohara, S. Nishiwaki, and T. Negami, "Characterization of the $Cu(In,Ga)Se_2$/Mo interface in CIGS solar cells," *Thin Solid Films*, vol. 387, no. 1-2, pp. 118–122, 2001.

[21] N. Kohara, S. Nishiwaki, Y. Hashimoto, T. Negami, and T. Wada, "Electrical properties of the $Cu(In,Ga)Se_2/MoSe_2$/Mo structure," *Solar Energy Materials and Solar Cells*, vol. 67, no. 1–4, pp. 209–215, 2001.

[22] L. Assmann, J. C. Bernède, A. Drici, C. Amory, E. Halgand, and M. Morsli, "Study of the Mo thin films and Mo/CIGS interface properties," *Applied Surface Science*, vol. 246, no. 1–3, pp. 159–166, 2005.

[23] H. Khatri and S. Marsillac, "The effect of deposition parameters on radiofrequency sputtered molybdenum thin films," *Journal of Physics Condensed Matter*, vol. 20, no. 5, Article ID 055206, 2008.

[24] G. Gordillo, F. Mesa, and C. Calderón, "Electrical and morphological properties of low resistivity Mo thin films prepared by magnetron sputtering," *Brazilian Journal of Physics*, vol. 36, no. 3, pp. 982–985, 2006.

[25] J. H. Scofield, A. Duda, D. Albin, B. L. Ballard, and P. K. Predecki, "Sputtered molybdenum bilayer back contact for copper indium diselenide-based polycrystalline thin-film solar cells," *Thin Solid Films*, vol. 260, no. 1, pp. 26–31, 1995.

[26] Z.-H. Li, E.-S. Cho, and S. J. Kwon, "Molybdenum thin film deposited by in-line DC magnetron sputtering as a back contact for $Cu(In,Ga)Se_2$ solar cells," *Applied Surface Science*, vol. 257, no. 22, pp. 9682–9688, 2011.

[27] W. Li, X. Yan, A. G. Aberle, and S. Venkataraj, "Analysis of microstructure and surface morphology of sputter deposited molybdenum back contacts for CIGS solar cells," *Procedia Engineering*, vol. 139, pp. 1–6, 2016.

[28] W. Li, X. Yan, A. G. Aberle, and S. Venkataraj, "Effect of deposition pressure on the properties of magnetron-sputter-deposited molybdenum back contacts for CIGS solar cells," *Japanese Journal of Applied Physics*, vol. 54, no. 8, Article ID 08KC14, 2015.

[29] C. Roger, S. Noël, O. Sicardy et al., "Characteristics of molybdenum bilayer back contacts for $Cu(In,Ga)Se_2$ solar cells on Ti foils," *Thin Solid Films*, vol. 548, pp. 608–616, 2013.

[30] C.-H. Huang, H.-L. Cheng, W.-E. Chang, M. Y. Huang, and Y.-J. Chien, "Investigation of sputtered Mo layers on soda-lime glass substrates for CIGS solar cells," *Semiconductor Science and Technology*, vol. 27, no. 11, Article ID 115020, 2012.

[31] J.-H. Yoon, K.-H. Yoon, W. M. Kim et al., "High-temperature stability of molybdenum (Mo) back contacts for CIGS solar cells: a route towards more robust back contacts," *Journal of Physics D: Applied Physics*, vol. 44, no. 42, Article ID 425302, 2011.

[32] S. S. Wang, C. Y. Hsu, F. J. Shiou, P. C. Huang, and D. C. Wen, "Properties of the Mo back contact for the formation of a thin-film photovoltaic absorber," *Journal of Electronic Materials*, vol. 42, no. 1, pp. 71–77, 2013.

[33] P. M. P. Salomé, J. Malaquias, P. A. Fernandes, and A. F. Da Cunha, "Mo bilayer for thin film photovoltaics revisited," *Journal of Physics D: Applied Physics*, vol. 43, no. 34, Article ID 345501, 2010.

[34] H.-M. Wu, S.-C. Liang, Y.-L. Lin et al., "Structure and electrical properties of Mo back contact for $Cu(In, Ga)Se_2$ solar cells," *Vacuum*, vol. 86, no. 12, pp. 1916–1919, 2012.

[35] D.-W. Lee, W.-J. Cho, J.-K. Song et al., "Failure analysis of $Cu(In,Ga)Se_2$ photovoltaic modules: degradation mechanism of $Cu(In,Ga)Se_2$ solar cells under harsh environmental conditions," *Progress in Photovoltaics: Research and Applications*, vol. 23, no. 7, pp. 829–837, 2015.

[36] Y. C. Kang, R. Khanal, J. Y. Park, R. D. Ramsier, H. Khatri, and S. Marsillac, "X-ray photoelectron spectroscopy investigation of oxidation states in molybdenum thin films for $Cu(InGa)Se_2$ applications," *Journal of Vacuum Science and Technology B:Nanotechnology and Microelectronics*, vol. 28, no. 3, pp. 545–548, 2010.

[37] S. A. Pethe, E. Takahashi, A. Kaul, and N. G. Dhere, "Effect of sputtering process parameters on film properties of molybdenum back contact," *Solar Energy Materials and Solar Cells*, vol. 100, pp. 1–5, 2012.

[38] T. Schlenker, V. Laptev, H. W. Schock, and J. H. Werner, "Substrate influence on $Cu(In,Ga)Se_2$ film texture," *Thin Solid Films*, vol. 480-481, pp. 29–32, 2005.

[39] J.-H. Yoon, W.-M. Kim, J.-K. Park, Y.-J. Baik, T.-Y. Seong, and J.-H. Jeong, "Control of the preferred orientations of $Cu(In,Ga)Se_2$ films and the photovoltaic conversion efficiency using a surface-functionalized molybdenum back contact," *Progress in Photovoltaics: Research and Applications*, vol. 22, no. 1, pp. 69–76, 2014.

[40] S. Chaisitsak, A. Yamada, and M. Konagai, "Preferred orientation control of $Cu(In_{1-x}Ga_x)Se_2$ ($x \approx 0.28$) thin films and its influence on solar cell characteristics," *Japanese Journal of Applied Physics*, vol. 41, no. 2, p. 507, 2002.

[41] M. Jubault, L. Ribeaucourt, E. Chassaing, G. Renou, D. Lincot, and F. Donsanti, "Optimization of molybdenum thin films for electrodeposited CIGS solar cells," *Solar Energy Materials and Solar Cells*, vol. 95, supplement 1, pp. S26–S31, 2011.

[42] K. H. Yoon, S. K. Kim, R. B. V. Chalapathy et al., "Characterization of a molybdenum electrode deposited by sputtering and its effect on $Cu(In,Ga)Se_2$ solar cells," *Journal of the Korean Physical Society*, vol. 45, no. 4, pp. 1114–1118, 2004.

[43] D. H. Shin, L. Larina, K. H. Yoon, and B. T. Ahn, "Fabrication of $Cu(In,Ga)Se_2$ solar cell with ZnS/CdS double layer as an alternative buffer," *Current Applied Physics*, vol. 10, no. 2, pp. S142–S145, 2010.

[44] J.-H. Yoon, S. Cho, W. M. Kim et al., "Optical analysis of the microstructure of a Mo back contact for $Cu(In,Ga)Se_2$ solar cells and its effects on Mo film properties and Na diffusivity," *Solar Energy Materials and Solar Cells*, vol. 95, no. 11, pp. 2959–2964, 2011.

[45] M. Theelen, K. Polman, M. Tomassini et al., "Influence of deposition pressure and selenisation on damp heat degradation of the $Cu(In,Ga)Se_2$ back contact molybdenum," *Surface and Coatings Technology*, vol. 252, pp. 157–167, 2014.